Experimental study of Natural convection flow in a cubic enclosure with a partially heated inner block

Alexandre Weppe, Florian Moreau, Didier Saury

▶ **To cite this version:**

Alexandre Weppe, Florian Moreau, Didier Saury. Experimental study of Natural convection flow in a cubic enclosure with a partially heated inner block. EUROTHERM2020 - 8th European Thermal Sciences Conference, Sep 2021, Lisbonne, Portugal. hal-03469756

HAL Id: hal-03469756
https://hal.science/hal-03469756

Submitted on 7 Dec 2021

HAL is a multi-disciplinary open access archive for the deposit and dissemination of scientific research documents, whether they are published or not. The documents may come from teaching and research institutions in France or abroad, or from public or private research centers.

L'archive ouverte pluridisciplinaire **HAL**, est destinée au dépôt et à la diffusion de documents scientifiques de niveau recherche, publiés ou non, émanant des établissements d'enseignement et de recherche français ou étrangers, des laboratoires publics ou privés.

Experimental study of a natural convection flow in a cubic enclosure with a partially heated inner block

Alexandre Weppe, Florian Moreau, Didier Saury

Institut Pprime UPR 3346, CNRS - ENSMA - Université de Poitiers,
Téléport 2, 1 avenue Clément Ader, BP40109, F-86961 Futuroscope Cedex, France

E-mail: alexandre.weppe@ensma.fr

Abstract. In many industrial contexts, buoyancy driven flows are the only cooling strategy in case of breakdown of the forced convection cooling system. In order to study those flows in a simplified configuration, a buoyancy-driven flow is generated inside a cubic enclosure by a partially heated block ($Ra = 1.4 \times 10^9$). The flow is studied experimentally in the vertical median plane, in the part of the enclosure where the flow is generated i.e. close to the heated side of the block. Velocity fields, mean profiles and RMS statistics are analyzed. The results show the presence of boundary layer flows with a central zone nearly at rest and stratified. RMS velocities are intensified with elevation.

1. Introduction

Turbulent and transient flows with dominant buoyancy effects are encountered in many industrial applications, especially in the nuclear or automotive sectors. For instance, the cooling of the engine compartment is a crucial point in the sizing of a vehicle. Following a sudden stop of the car vehicle after a heavy load, its integrity must be preserved even when it is no longer cooled by a forced external flow. For such situations, natural convection, often in turbulent regimes, ensures cooling.

This experimental study is part of a project which aims to solve the problems encountered by industrial partners during numerical simulations of turbulent flows with dominant buoyancy effects in a confined enclosure. Its purpose is also to improve the understanding of the physical phenomena behind those flows.

A simplified configuration is defined and used to study a natural convection flow with similar regimes to those observed in the under-hood of cars. In this study, a cubic enclosure with a partially heated inner block represents the engine. Several studies, mostly numerical, deal with the influence of an obstacle inside a cavity. Some studies show the impact of the size and conductivity of an unheated block [1, 2] while others focus on the role of a heated block on combined conduction/convection transfers [3, 4]. As it will be seen in this paper, the part of the flow studied in the present work has some properties similar to the flows observed in a differentially heated cavity. Turbulent flows generated in a closed differentially heated cavity have already been studied experimentally [5, 6, 7]. This paper aims to understand the dynamical behavior of the flow in the heated channel of this simplified configuration.

2. Experimental apparatus and metrology

2.1. Experimental apparatus

The configuration studied consists in a cubic enclosure with sides of length $L = 1\,\mathrm{m}$ in which a cubic heated block of length $H_{bloc} = 0.8\,\mathrm{m}$ is placed (Fig. 1). A temperature $T_c = 292\,\mathrm{K}$ is imposed on two of the side walls of the cubic enclosure by two aluminium/water heat exchangers with thermostated baths (conductivity $\lambda = 174\,\mathrm{W.m^{-1}.K^{-1}}$). Top and bottom horizontal walls are made of extruded polystyrene (conductivity $\lambda = 0.035\,\mathrm{W.m^{-1}.K^{-1}}$) and are considered as adiabatic. They are covered with a low-emissivity Mylar sheet ($\epsilon = 0.044$). The front and rear walls are glass panels of width 6 mm. Extruded polystyrene panels are maintained in front of those walls to preserve their adiabatic roles. Still, a space is reserved for the visualization.

The cubic block inside the enclosure is maintained by four polymer supports attached to threaded rods. It is composed of two 4 cm thick aluminium plates (conductivity $\lambda = 174\,\mathrm{W.m^{-1}.K^{-1}}$). One of them is heated (left one on Fig. 1b) by a resistive wire at a temperature $T_h = 325\,\mathrm{K}$ and the other one (right one on Fig. 1b) is considered as inert. Rockwool panels with POM-C and Ertalon plates are placed between the two aluminium plates. Top, bottom, front and rear block faces are covered with 4 mm thick POM-C plates to ensure good roughness conditions. These plates are covered with a low-emissivity Mylar sheet.

The Rayleigh number based on the block's length is $Ra_{H_{bloc}} = \frac{g\beta\Delta T H_{bloc}^3}{\alpha\nu} = 1.4 \pm 0.03 \times 10^9$. It is obtained with a temperature difference between the heated plate of the cubic block and the enclosure's side wall: $\Delta T = T_h - T_c = 33 \pm 1\,\mathrm{K}$. The working area is defined in Fig. 1a.

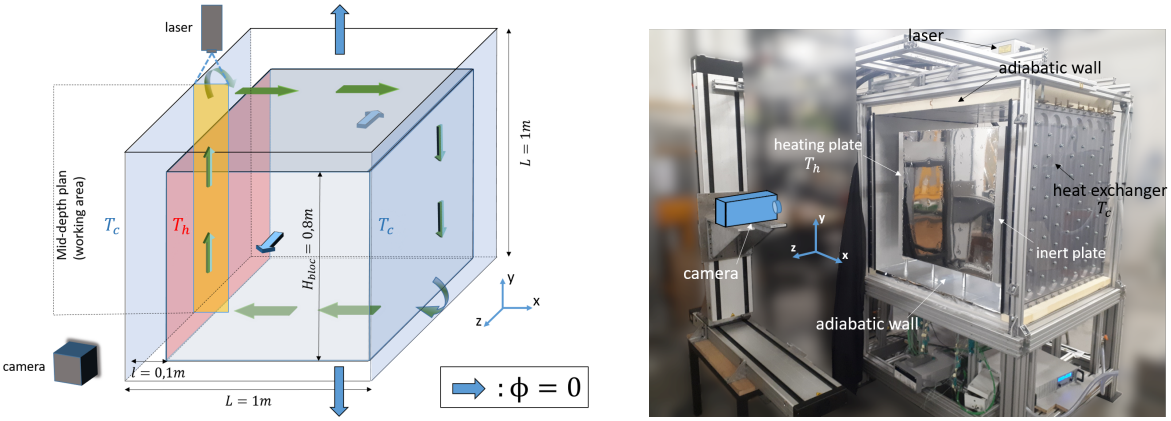

(a) (b)

Figure 1: a): 3D configuration with working area b): experimental apparatus

2.2. Velocity measurements

Velocities have been measured by PIV. A smoke generator produces the flow tracer (paraffine oil particles : $\rho_p = 856\,\mathrm{kg.m^3}$, $d \approx 5\,\mu\mathrm{m}$ (diameter), $Stk = \frac{\rho_p d^2 v_{ref}}{18\mu l} = 6.2 \times 10^{-4}$ (Stokes Number) where $v_{ref} = \frac{\alpha}{H_{block}}\sqrt{Ra_{H_{block}}}$ and the laser sheet is generated by a pulsed laser Nd:YAG Litron. The particles are a good air tracer since $\frac{V_g}{V_{max}} \approx 1.5 \times 10^{-3}$ where $V_g = \frac{d^2 g(\rho_p - \rho_{air})}{18\mu}$ is the settling velocity. The particles are visualized with a camera Tokina F100 of resolution $2320 \times 1720\,\mathrm{pixels}^2$. The pixel size is $7\,\mu\mathrm{m}$ and the field size is set to $97 \times 72\,\mathrm{mm}^2$.

6000 pairs of images are acquired at 96 Hz and the time between two images is ranged between 1000 and 5000 μs depending on the visualized zone. 17 zones are visualized and intersected when necessary. For each zone, vertical and horizontal mean and RMS velocities are analyzed. Image processing is carried out with the "Adaptative PIV" algorithm from Dantec. This algorithm

adapts interrogation areas size (from 64×64 to 32×32) to be more precise in zones where particle density is sufficient. The overlapping varies between 75% and 50%. The velocity uncertainty is approximatively $0.005\,\mathrm{m.s^{-1}}$ (method described in [8]).

3. Results

Measurements have been carried out in the vertical mid-depth plane in the working area defined in figure 1a. Figure 2a shows vertical velocity fields and velocity vectors for the working area at $Ra_{H_{bloc}} = 1.4 \times 10^9$. Mean velocity profiles have also been plotted for different elevations along the working area (figures 2b and 2c) with the origin $y = 0\,\mathrm{mm}$ taken on enclosure bottom wall. Velocity profile positions are drawn Fig. 2a. The flow is ascending along the hot wall (at temperature T_h) and a boundary layer flow is observed. The boundary layer thickens from the beginning of the hot wall to its end (Fig. 2a). There is no more boundary layer when the flow is not anymore in contact with the wall ($y \leq 100\,\mathrm{mm}$ and $y \geq 900\,\mathrm{mm}$). A very weak descendant boundary layer flow is also observed along the cold wall (at temperature T_c) but is less thick than the ascendant one. The absolute maximum velocity for the descendant boundary layer flow is approximately four times inferior to the one for the ascendant flow (for $y = 593\,\mathrm{mm}$: $V_{max} = 0.360\,\mathrm{m.s^{-1}}$, $V_{min} = 0.085\,\mathrm{m.s^{-1}}$). In fact, a part of the ascendant flow goes to the top canal as it is shown with the mean horizontal velocities U for $y = 957\,\mathrm{mm}$, where ($U(x = 97\,mm) > 0$) and the velocity vectors (figures 2a and 2c).

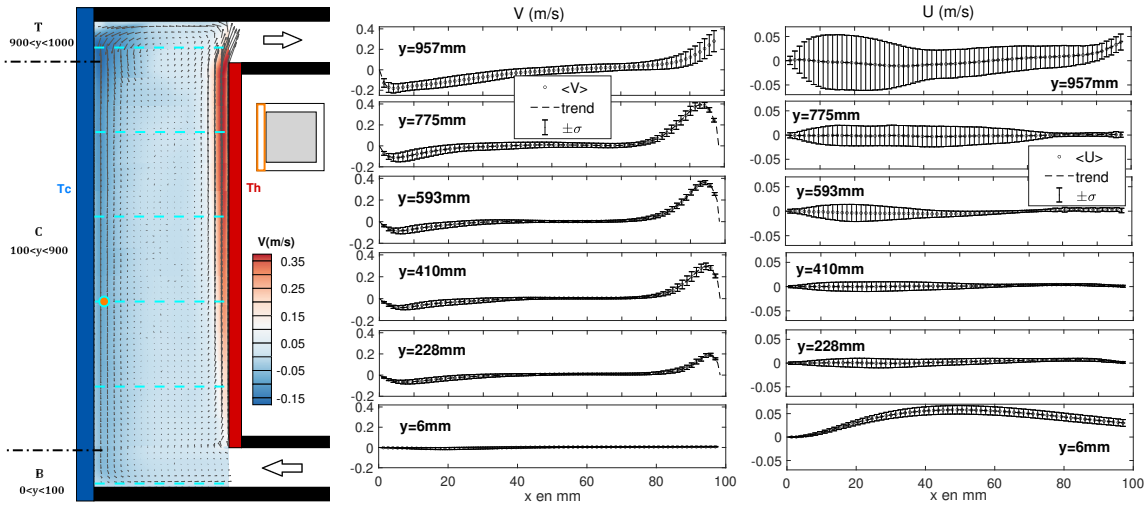

(a) (b) (c)

Figure 2: a):Vertical velocity fields, dotted line profiles and orange point for the spectral study b): Vertical component of velocity profiles c): Horizontal component of velocity profiles.

For areas with boundary layer flows (refered as area C in Fig. 2a), mean horizontal U and vertical V velocities in the central zone of the area are close to 0. Nonetheless, RMS values of the horizontal components of the velocity (corresponding to the envelope over mean velocities and of 2σ height in figures 2b and 2c) near the cold wall and the central zone increase with the elevation and are higher than those near the hot wall. Indeed, the vertical velocity in the ascendant boundary layer is high and thus the boundary layer is not destabilized horizontally. Considering the velocity vectors, multiple situations are observed. In the bottom zones considered (area C bottom), a part of the flow coming from the descendant boundary layer crosses the central zone and feeds the emerging ascendant boundary layer flow. In central zones (area C middle), flow directions are more complex but the corresponding velocities are very low and do not contribute much to the mean mass transfer. Areas B and T (Fig. 2a) have no wall at $x = 97\,\mathrm{mm}$. Then,

for the B area, a part of the descendant flow goes to the bottom canal as the velocity vectors show in Fig. 2a. The other part of the flow feeds the ascendant boundary layer. At $y = 6\,\text{mm}$, horizontal velocities U are positive. On the contrary, and due to the flow near the bottom wall, vertical velocities V are close to zero. For the T area, velocity vectors show that a part of the flow goes to the top enclosure canal. It also explains why the horizontal velocities observed are positive near $x = 97\,\text{mm}$ for $y = 957\,\text{mm}$. The other part of the flow rises up to the adiabatic top wall enclosure and then goes back to the cold wall before flowing through the descendant boundary layer. A large vortex is observed near the top corner.

Power spectral density and time response are plotted for the horizontal velocity at a point inside the descendant boundary layer and drawn on figure. 2a ($x = 14\,\text{mm}$, $y = 410\,\text{mm}$). The spectral density observed tends to notably decrease from the frequency ($f = 1\,Hz$) and follows a linear equation of slope -3 (Fig. 3). This coefficient represents the effects of the buoyancy forces on the turbulence scales decrease in the inertial zone [9]. Power spectral density in this zone does not depend on viscosity as it is generally observed for a flow without buoyancy forces influence. A slope of $-5/3$ should be observed in that case.

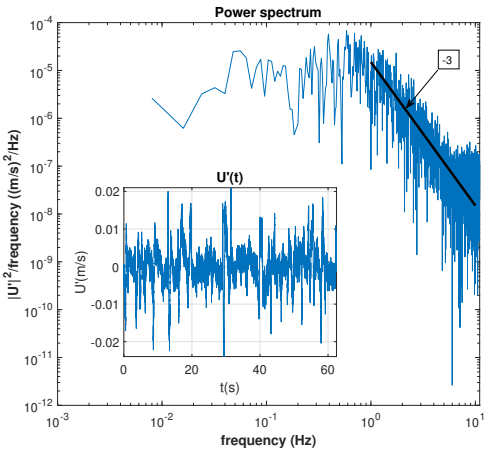

Figure 3: Power spectrum and U' vs t for the point drawn on Fig. 2a.

4. Conclusion

This study characterized the flow topology inside an enclosure at $Ra_{H_{bloc}} = 1.4 \times 10^9$. Velocity measurements have been carried out in the vertical mid-depth plane. Two boundary layer flows and a central zone nearly at rest have been observed. RMS values of the velocities in the central zone and near the cold wall are highlighted. The global circulation of the flow has also been studied. In the end, the buoyancy forces effect has been shown with the spectral study of a point in the descendant boundary layer.

References

[1] House J M, Beckermann C and Smith T F 1990 *Numerical Heat Transfer, Part A: Applications* **18** 213–225
[2] Bhave P, Narasimhan A and Rees D A S 2006 *International Journal of Heat and Mass Transfer* **49** 3807–3818
[3] Liu Y and Phan-Thien N 1999 *Computational Mechanics* **24** 175–186
[4] Ha M Y and Jung M J 2000 *International Journal of Heat and Mass Transfer* **43** 4229–4248
[5] Saury D, Rouger N, Djanna F and Penot F 2011 *Int. Com. in Heat and Mass Transfer* **38** 679–687
[6] Salat J, Xin S, Joubert P, Sergent A, Penot F and Le Quéré P 2004 *Int. J. of Heat and Fluid Flow* **25** 824–832
[7] Betts P L and Bokhari I H 2000 *International Journal of Heat and Fluid Flow* **21** 675–683
[8] Guillaume G, Beaulieu C, Braud P and David L 2018 Démarche d'estimation des incertitudes en PIV basée sur la méthode GUM *16ème Congrès Francophone de Techniques Laser pour la mécanique des fluides*
[9] Gebhart B and Jaluria Y 1988 *Buoyancy-Induced Flows And Transport* (Taylor & Francis)